Electronic Supplementary Information

A fluorescent biosensor based on long-range self-assembled DNA cascades and upconversion nanoparticles for the detection of breast cancer-associated circulating microRNA in serum samples

Jianming Lan[a], Fadi Wen[b], Fangmeng Fu[c], Xi Zhang[b], Shuxian Cai[b], Zhijing Liu[b], Dongzhi Wu[b], Chunyan Li*[,a] JingHua Chen*[b],*Chuan Wang*[c]

Received (in XXX, XXX) Xth XXXXXXXXX 200X, Accepted Xth XXXXXXXXX 200X
DOI: 10.1039/b000000x

[a] Department of Basic Chemistry, Faculty of Pharmacy, Fujian Medical University, Fuzhou, Fujian 350108, P R China

[b] Department of Pharmaceutical Analysis, Faculty of Pharmacy, Fujian Medical University, Fuzhou, Fujian 350108, P R China

[c] Department of breast surgery, Fujian Medical University Union Hospital, Fuzhou, Fujian 350001, P R China.

1. Experimental parts

1.1 Reagents and Apparatus

Yttrium oxide (99.99%), ytterbium oxide (99.99%) and erbium oxide (99.99%) were purchased from FengYue Chemicals co., Ltd (Tianjin, China). Dimercaptosuccinic acid (DMSA), Dimethylsulfoxide (DMSO) and stearic acid were obtained from Sinopharm Chemical Reagent Co., Ltd (Shanghai, China). Oleic acid (OA), 1-Octadecene (ODE) and NaF were purchased from Aladdin Reagent co., Ltd (Shanghai, China). DNA and RNA sequences were purchased from Sangon Biotech co., Ltd (Shanghai, China) and were illustrated in Table S1.

Table S1 Details of the DNA sequences

Capture probe (CP):	5′-biotin-GGCCGTCAACATCAGTCTGATAAGCTAAACATGATGACGGCC-3′
Target miRNA-21:	5′-UAGCUUAUCAGACUGAUGUUGA-3′
Auxiliary probe1 (AP1):	5′-GCACCTGGGGGAGTAAGTGGCCGTCATCAT-3′
Auxiliary probe2 (AP2):	5′-TACTCCCCCAGGTGCATGATGACGGC CACT-NH_2-3′

Single-base mismatch target(1MT):	5′-UAGCUUAUCGGACUGAUGUUGA-3′
Two-base mismatch target (2MT):	5′-UAGCUUAUCGGACUCAUGUUGA-3′
Noncomplementary sequence (NC):	5′-AAAAAAUCUGCUGAGGAUAAAA-3
miRNA-155:	5′-UUAAUGCUAAUCGUGAUAGGGGU-3′
miRNA-16:	5′-UAGCAGCACGUAAAUAUUGGCG-3′

X-ray powder diffraction (XRD) measurements were performed on Mini Flex Ⅱ X' Pert Pro diffractometer (Riguka Co., Japan) with graphite monochromatized Cu Kα radiation (λ=0.15406 nm). The size and morphology of as-prepared nanoparticles were observed by a JEM-1200EX transmission electron microscope (TEM, JEOL Ltd., Japan) equipped with an electron diffractometer (ED). Fourier transform infrared (FT-IR) spectra of UCNPs-COOH were measured on Spotlight 400/400N spectrometer (Perkin Elmer Co., USA) by the KBr method. The upconversion (UC) fluorescent spectra were recorded with a Cary Eclipse fluorescence spectrophotometer (Varian Co., USA) attached an external 980 nm laser (CNI Co., China) instead of internal excitation source.

1.2 Synthesis of hydrophobic $NaYF_4$: Yb^{3+}/Er^{3+} UCNPs

Firstly, the rare earth stearates $(C_{17}H_{35}COO)_3RE$ (RE = $Y_{0.78}Yb_{0.20}Er_{0.02}$) were synthesized by reacting RE oxides with stearic acid according to the related literature [1]. Then $NaYF_4$:Yb^{3+}/Er^{3+} nanocrystals were synthesized by thermal decomposition of rare-earth stearates as precursors in OA-ODE system as reported previously [2]. In a typical procedure, 1.0 mmol of rare earth stearates were dissolved in a 100 ml three-necked flask with existence of OA (10 mL) and ODE (10 mL). After adding 12 mmol NaF, the mixture was then heated to 100 °C with vigorous stirring under vacuum for 60 minutes to form a clear solution. Afterwards, the solution was heated to 310 °C at

a rate of 20 °C/min and maintained at 310 °C for 60 minutes to obtain the UCNPs. The UCNPs were deposited by adding cyclohexane/ethanol (1:1 v/v) solution and separated via centrifugation. The resulted UCNPs were further purified by dispersing in a minimum amount of chloroform and deposited with excess ethanol and finally dried under vacuum for 24 h.

1.3 Surface modification of $NaYF_4$: Yb^{3+}/Er^{3+} UCNPs

In a typical procedure [3], 0.20 g hydrophobic nanoparticles of $NaYF_4$:Yb^{3+}/Er^{3+} were dispersed in 10 mL toluene. Afterwards, 10 mL DMSO solution (including 0.15 g DMSA) was injected into above solution. After magnetic stirring for 3 h, the as-prepared products were collected by centrifugation and washed with ethanol several times, finally dried under vacuum in low temperature.

1.4 Influence of the temperature on the PL intensity of UCNPs

The 1.0×10^{-4} mol/L $NaYF_4$:Yb^{3+}/Er^{3+}-COOH aqueous solution was prepared according to stoichiometric coefficient. The fluorescence spectra of the solution were investigated by Cary-50 fluorescence spectrophotometer using exciting light of 980 nm under the temperature of 20°C, 30°C, 35°C, 40°C, 45°C, 50°C, 60°C, 70°C, respectively.

1.5 Coating of avidin in microplate and fixation of CP probes.

$NaYF_4$:Yb^{3+}/Er^{3+}-COOH nanocrystals were crosslinked on AP2 according to the reference [4]. In this process, 1-Ethyl-3- (3-dimethyllaminopropyl) carbodiimide hydrochloride (EDC) and N-Hydroxysulfosuccinimide sodium salt (NHS) were added to 1mL phosphate buffer solutions (PBS) buffer (0.3M), and the mixture with the

concentration of 0.1 M was obtained by stirring. Then 2 mg $NaYF_4:Yb^{3+}/Er^{3+}$-COOH nanocrystals were added to the above mixture under rapid stirring. Finally 100 μL AP2 (10μM) was added to the above mixture under vigorous stirring at room temperature, and the mixture solution was stirred sequentially for two hours. The obtained solution was preserved at 4℃.

Every pore plate was coated with 100 μL avidin, which was diluted by carbonate buffer (pH 9.0). The coating reaction was processed at 4 ℃ for 12 h. Then the microplate was rinsed several times by PBS buffer and dried. Finally, the microplate was sealed off with 3% bovine serum albumin (BSA). Before the fixation of CP, CP were heated to 95 ℃ for 10 min and naturally cooled to room temperature. Then 10 μM CP were transferred to the microplate and kept under 25℃ for 30 min. Finally, the residuals were poured out and the microplate was rinsed by PBS and baked.

1.6 The sensor detection of target sequence T1

The 100μL target miRNA was transferred to the microplate fixed with CP. The above microplate was incubated at room temperature for 120 min after adding hybrid buffer. Then the residuals were poured out, and the microplate was rinsed by PBS and baked. Finally, 1μM AP1 and 1μM AP2 modified with $NaYF_4:Yb^{3+}/Er^{3+}$-COOH nanocrystals were transferred to the microplate and kept under 25 ℃ for 120 min. Then the residuals were poured out, and the microplate was rinsed by PBS and baked. The fluorescence spectra were investigated by Cary-50 fluorescence spectrophotometer using exciting light of 980 nm after adding 100 μL buffer into every microplate.

2. Results and discussions

2.1 Characterization of the $NaYF_4:Yb^{3+}/Er^{3+}$ UCNPs

The TEM images, XRD pattern, FT-IR spectrum and fluorescence spectrum of the $NaYF_4:Yb^{3+}/Er^{3+}$ UCNPs are shown in Fig. S1 and Fig. S2. The TEM images (Fig. S1 a, b) show that the particles are roughly spherical, highly monodisperse, uniform, and narrow in size distribution with a mean diameter of about 25 nm. High-resolution TEM (HRTEM) measurements (Fig. 1c) reveal that the as-prepared UCNPs are of single crystalline nature. The selected-area electron diffraction (SAED) pattern (Fig. 1d) shows spotty polycrystalline diffraction rings corresponding to the (100), (101), (110), (111), (201), (211), (311) ,and (410) planes of the β-phase NaYF4 lattice. We can also clearly distinguish the lattice fringes on individual UCNPs from the HRTEM images. The value 0.517 nm between the lattice fringes correspond to the d spacing for the (100) lattice planes.

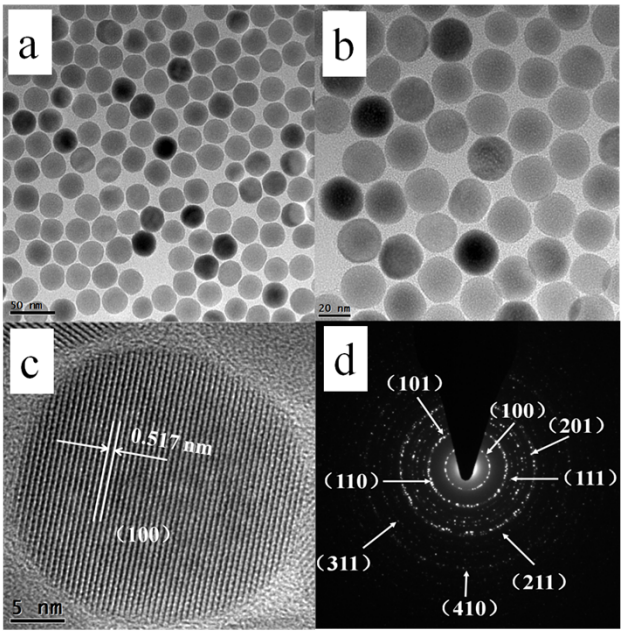

Fig. S1 (a, b) TEM images of the NaYF4:Yb^{3+}/Er^{3+} UCNPs; (c) HRTEM images of

UCNPs; (d) SAED pattern of UCNPs.

The XRD pattern (Shown as Fig. S2 a) agrees well with the standard pattern of the hexagonal phase $NaYF_4$ (JCPDS No. 028-1192), suggesting the pure hexagonal phase and high crystallinity of the nanoparticles. Fig. S2 b shows that there are three emission peaks at 524 nm, 541 nm and 657 nm, which are assigned to the $^2H_{11/2} \rightarrow {}^4I_{15/2}$, $^4S_{3/2} \rightarrow {}^4I_{15/2}$ and $^4F_{9/2} \rightarrow {}^4I_{15/2}$ transitions of Er^{3+} ions, respectively. The emission peak at 657 nm was chosen as the testing signal in our detection, which is the strongest peak.

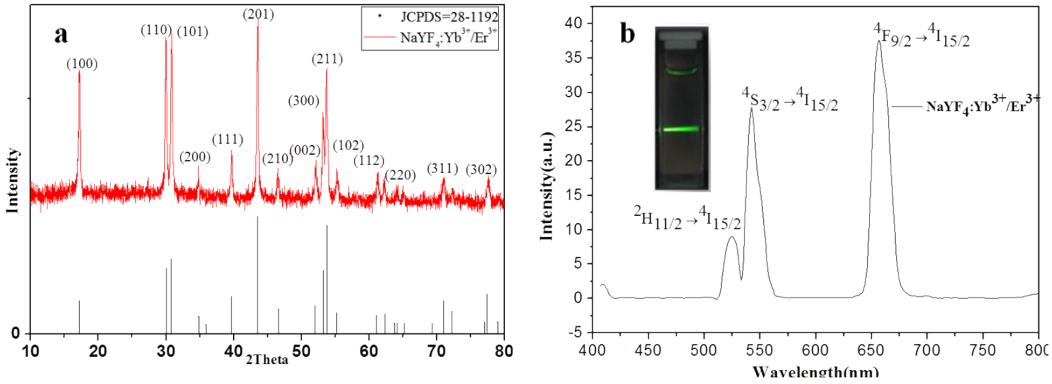

Fig. S2 Characteristics of synthesized $NaYF_4$:Yb^{3+}/Er^{3+} UCNPs. (a) Experimental powder XRD pattern (top curve) and the calculated line pattern (bottom curve) for β-NaYF4 (JCPDS No. 028-1192). (b) Upconversion fluorescence spectrum. (Inset: The photograph under 980 nm laser illumination)

Fig. S3 presents the IR spectrum of the $NaYF_4$: Yb^{3+}/Er^{3+} UCNPs after surface modification. Due to some strong hydrogen bonds, the carboxylic acid groups exist in the form of dimers under solid state. The strong band in the range of 3300-2500 cm^{-1} corresponds to the O-H stretching vibration, while the weak peaks at 2954 and 2921 cm^{-1} are related to the stretching vibration of the C-H bond, overlaying in the range of

O-H stretching vibration. The very weak band at 1718 cm^{-1} can be assigned to the asymmetric stretching vibrations of the C=O group. Because hydrogen bonds and resonance weaken the C=O bond, so the absorption frequency of the C=O bond in dimer is lower than that in monomer. Carboxylic acid anion has two strong coupling bonds of carbon-oxygen, the peaks attributed to the strong asymmetric stretching vibrations and the weak symmetric stretching vibrations can be seen at 1610 and 1415 cm^{-1}, respectively. The S-H bond can't be found in this IR spectrum, which is particularly weak. These data indicated that the UCNPs are capped with a layer of DMSA, rendering the nanoparticles hydrophilic and readily dispersible in water.

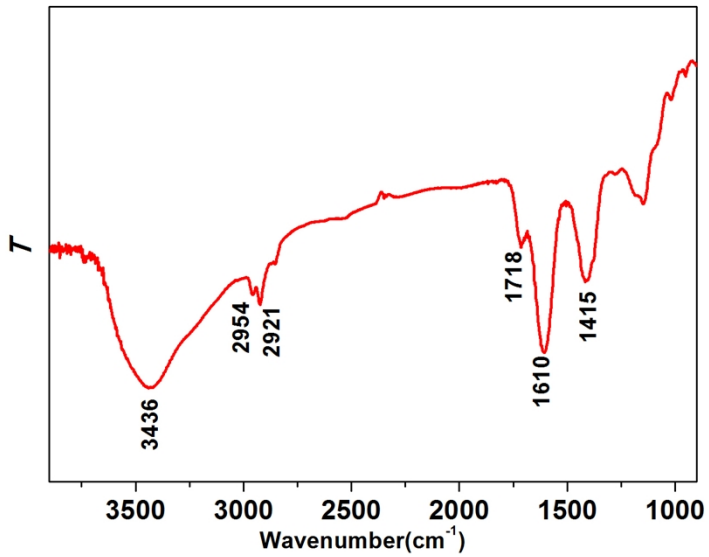

Fig. S3 IR spectrum of $NaYF_4$:Yb^{3+}/Er^{3+}-COOH UCNPs.

2.2 Influence of the temperature on the PL intensity of UCNPs

During our experiments as shown in Fig.S4 in ESI, the results show that the PL intensity has small change in the physiological range between 20 and 45 °C, but the PL intensity increase obviously when the temperature is higher than about 50 °C. So we chose 25 °C as test temperature.

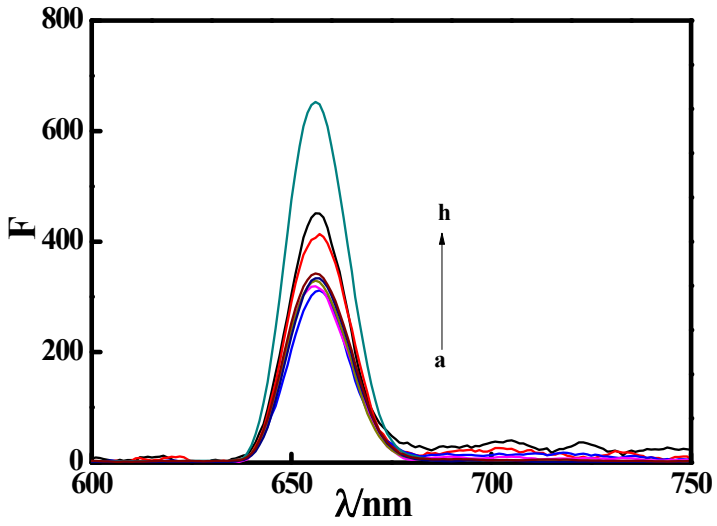

Fig. S4 Influence of the temperature on the PL intensity of UCNPs. From a to h is 20°C, 30°C, 35°C, 40°C, 45°C, 50°C, 60°C, 70°C, respectively.

2.3 Selectivity, stability of the biosensor

To examine the selectivity of our proposed amplified biosensor, we performed a comparison study on mismatch targets and perfect complementary target. Fig.S5 shows the fluorescence intensity for the different kinds of targets including the perfect complementary target miR-21 at a concentration of 1 pM and single-base mismatch target (1 MT), two-base mis-match target (2 MT), and non-complementary sequence (NC), each with concentration of 1nM. As expected, single-base mismatch target results in 8.9 % increasing of the fluorescence intensity (57.7 a.u.) compared to blank treatment (0 %, 0.1 a.u.) and perfect complementary target miR-21 (100 %, 648.6 a.u.). Additionally, using the two-base mismatch target causes 5.2 % increasing of the fluorescence intensity (33.5 a.u.), whereas the non-complementary sequence leads to only 2.0 % increasing of the fluorescence intensity (13.0 a.u.). These results demonstrate that our proposed biosensor shows high selectivity for the perfect

complementary target miR-21. In reality, the method should be able to distinguish the target miRNA from other miRNAs for complex mixture.

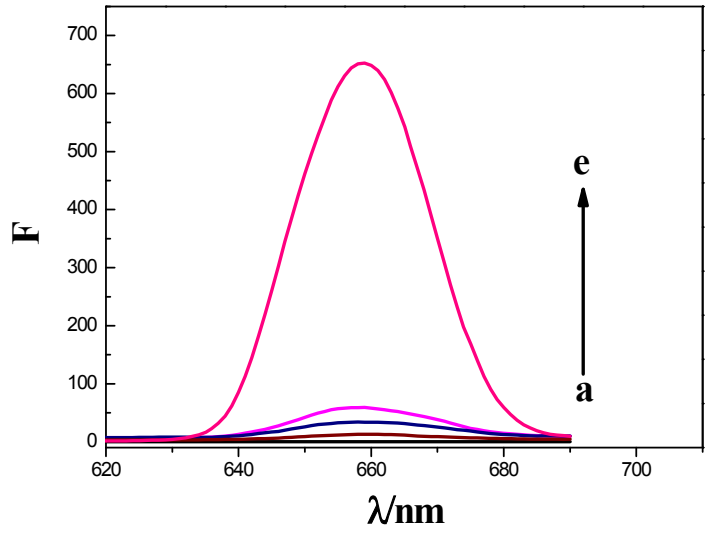

Fig. S5 Fluorescence intensity for the blank and the four various RNA sequences:(a) blank, (b)NC, (c) 2MT ,(d) 1MT,and (e) target miR-21.The concentrations of 1MT, 2MT, and NC were 1nM. The concentration of target miR-21 was 1pM.

Thus we selected the target miR-21 and two other miRNAs (miRNA-155 and miRNA-16) as study object to evaluate the effectiveness of an affinity assay in analyte detection by similar assay procedure. As shown in Fig.S6, both miR-155 and miR-16 generated insignificant fluorescent changes compared to the perfect match target miR-21. The fluorescence intensity of miR-21 was approximately 30 fold higher than that of miR-155 and miR-16. These results suggest that the proposed method with high sequence specificity has a potential application in discriminating differences of miRNA sequence. In this work, the stability of the biosensor was also investigated. The modified pore plate, which was immersed in buffer and stored at 4

℃ for 24 h, could still be used for the measurement of target miR-21 without significant change of fluorescence response. Thus, the developed biosensor shows good stability within 24 h.

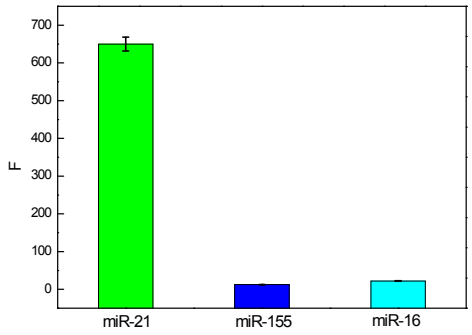

Fig. S6 Specificity of miRNA assay. Bars represent the fluorescence F from the different inputs of miR-21, miR-155 and miR-16. The concentration of target miR-21 was 1 pM, miR-155 and miR-16 with the same concentration of 1 nM.

2.4 Determination of miR-21 in human serum samples

The standard adding method was used to determine miR-21 in the breast cancer patient's serums. We choose a cancer patient serum sample as an example. A series of synthetic miR-21 at concentrations of 10,15, 20, 25, 30, and 45 fM were spiked into serum sample, respectively, with equal volume to establish a calibration curve (in this case, the concentration of serum sample and synthetic miR-21 were both equivalent to be diluted 2-fold). The other steps were followed by the same experimental procedures described in experimental section.

As shown in Fig. S7, the fluorescent intensities of the system increased with the increasing of the spiked concentration of the synthetic miR-21 and exhibited a fairly good linear relationship in the range from 10 to 45 fM (Shown as inset of Fig.S7).

According to the standard addition method, the concentration of miR-21 in the diluted serum sample was estimated to be 2.1 fM. Thus, the content of miR-21 in the original serum sample was calculated to be 4.2 fM.

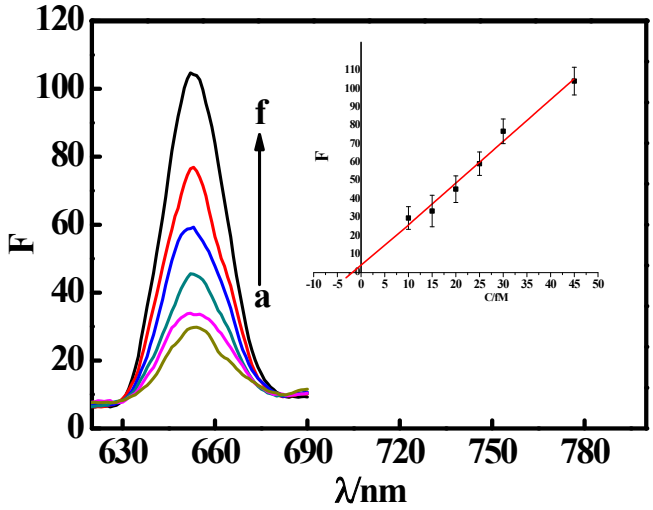

Fig.S7 Variation diagram of fluorescence intensity with the different concentrations of miR-21. (a) 10 fM (b) 15 fM (c) 20 fM (d) 25 fM (e) 30 fM (f) 45 fM (Inset: linear graph for fluorescence intensity with the concentrations of miR-21)

References

[1] Wang, M., Liu, J. L., Zhang, Y. X., Hou, W., Wu, X. L., Xu. S. K., J. Mater. Lett., 2008, **63**, 325.

[2] Li, C. X., Lin, J. J., J. Mater. Chem., 2010, **20**, 6831.

[3] Chen, Q. T., Chen, F. H., Liu, G. X., Dong, X. T., Wang, J. X., Sci. China-Chem., 2011, **41**, 798.

[4] Bath J., Thrberfield A., Nat. Nanotechnol., 2007, **2**，275.